GEOLOGICA CARPATHICA, DECEMBER 2006, 57, 6, 461–472

Silicification of quartz arenites overlain by volcaniclastic deposits: an alternative to silcrete formation

KAREL D. MALÝ[1,2,3], VLADIMÍR CAJZ[1], JIŘÍ ADAMOVIČ[1*] and JIŘÍ ZACHARIÁŠ[2]

[1]Institute of Geology, Academy of Sciences of the Czech Republic, Rozvojová 269, 165 02 Praha 6, Czech Republic; maly@gli.cas.cz; cajz@gli.cas.cz; *✉ adamovic@gli.cas.cz
[2]Faculty of Science, Charles University, Albertov 6, 128 43 Praha 2, Czech Republic; zachar@natur.cuni.cz
[3]Czech Geological Survey, Geologická 6, 152 00 Praha 5, Czech Republic

(Manuscript received December 8, 2005; accepted in revised form March 16, 2006)

Abstract: The origin of the flat-lying body of quartzite at Skalice near Litoměřice, Ohře Rift graben, Bohemian Massif, is explained by the effect of emplacement of dense tuff of tephritic mineral composition on Eocene quartz sands. In the upper part of the ca. 10 m thick quartzite body, broad quartz overgrowths on detrital grains are visible in CL images, with individual zones/bands having variable Al contents. The lower part of the quartzite body features isopachous growth bands with less variation in Al contents, passing to euhedral quartz precipitation. Porosity of the quartzite decreases upwards, reaching 3.8 % below the tuff base. Two main silicification stages are inferred: 1. dealkalization of the tuff and volcanic glass recrystallization, reflected in isopachous precipitation of poorly crystalline silica in deeper parts of the quartzite profile from fluids with high silica concentration and high amount of impurities; 2. hydrothermal argillization of the basal tuff portions connected with the origin of euhedral quartz cement deeper in the quartzite profile and opal coatings in shallower parts of the profile. Simple mass balance calculation shows that the tuff itself could not produce much silica for the underlying quartzite, and that most silica was produced by the corrosion and dissolution of sand grains by alkaline fluids in a zone immediately underlying the tuff. The Skalice quartzite should be viewed as a product of hydrothermal silicification rather than silcretization.

Key words: Ohře Rift, dealkalization, silicification, silcrete, dense tuff, quartz overgrowths, quartzite.

Introduction

The process of silicification in sedimentary formations of different age and different lithological composition produces SiO_2-rich rocks — quartzites. This process involves leaching of SiO_2 from silica-rich minerals, its transport in solution driven by thermal gradient or gravity, and its precipitation. Even in high-permeability rocks, this process is multiphase rather than instantaneous, giving rise to characteristic mineral sequences.

Silica solubility increases in the presence of ferric iron, and with increasing amounts of salts and dissolved organic compounds (Thiry 1997). In solutions, silica tends to get oversaturated with decreasing pH and/or decreasing temperature. The phases precipitated are controlled by the character of the host rock, prevailing pore-water chemistry, SiO_2 saturation and the presence of ion impurities.

In general, sedimentary quartzite bodies of three different genetic types can be encountered in natural environments: diagenetic quartzites formed in deeply buried sedimentary formations, hydrothermal quartzites formed at/near the contact with magmatic bodies, and silcretes formed by atmospheric effects near the Earth's surface.

The term "silcrete" has been rather loosely used for quartzites of various origins in the past. Here, we reserve this term for quartzite formed by silica concentration at or near the Earth's surface under specific physicochemical conditions and low temperatures. Two main types are distinguished. Pedogenic silcretes are typical for regions with distinct wet and dry periods, and form thin layers with columnar structures (Summerfield 1983). Vertical zoning ranges from megaquartz at the top, microquartz in the middle and opal at the base (Thiry 1997). These features are compatible with dominant downward movement of fluids. Groundwater silcretes originate near the groundwater table and show less distinct vertical differentiation: quartz overgrowths in pure sands and amorphous or fibrous silica formation by replacement of clay minerals (Thiry & Milnes 1991).

Dissolved silica is a common constituent of hydrothermal fluids. It is either leached from lavas and pyroclastic deposits, especially glass, upon their cooling or from ambient silica-rich rocks. Sinters and pore fillings formed by opal and chalcedony are dominant in modern geothermal fields, such as those in Wyoming (Yellowstone) and New Zealand (Kawerau and Taupo–Rotorua). A strong contribution of microbes to opal precipitation is typical for such settings (Guidry & Chafetz 2003).

The genesis of ancient siliceous deposits can be partly deciphered by the geological position of the quartzite bodies in question, their geometry and their relation to the paleosurface. While subvertical quartzite bodies can generally be attributed to the action of hydrothermal systems, the situation is more complicated with subhorizontal bodies. Here, silicification may be controlled by hydrothermal fluid flow following a subhorizontal body of high-permeability sediment, but may equally be of epigenetic origin.

Subhorizontal quartzite bodies hosted by quartz arenites are a common feature in the area of the Ohře Rift, a taphro-

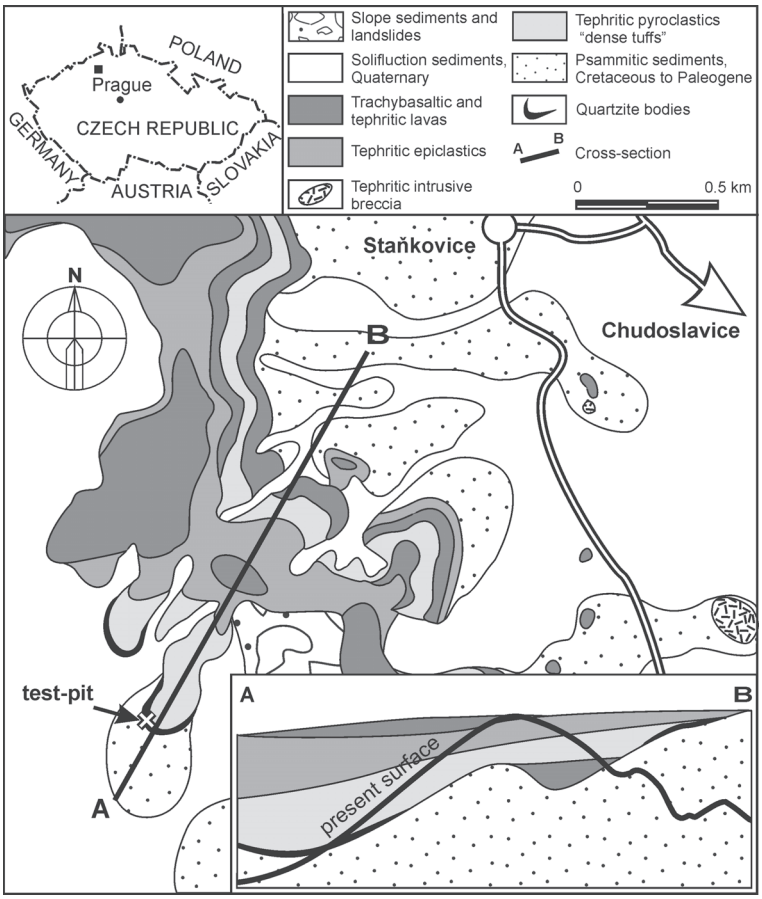

Fig. 1. The distribution of dense tuff at Dlouhý vrch Hill near Litoměřice with indicated location of the test-pit excavated in the Skalice quartzites near the tuff base. Vertical dimension of cross-section A–B is exaggerated by the factor of 2.7.

genic structure in the western part of the Bohemian Massif pertaining to the European Cenozoic rift system (Prodehl et al. 1995). They have generally been interpreted as products of tropical weathering (pedogenic and groundwater silcretes), for example by Kužvart (1965) and Malkovský (1985, 1991) as they are often associated with products of kaolinization and are of large areal extent. Some quartzite bodies of smaller extent are, however, overlain by altered pyroclastic material; this may equally suggest their hydrothermal/metasomatic origin (Dittler & Hibsch 1928). A revision of a typical occurrence of the latter type is the subject of this study.

Geological setting

The type locality of the Skalice quartzites is situated at Dlouhý vrch Hill near Skalice, north of Litoměřice, on the SE slope of the volcanic range of the České středohoří Mts (Fig. 1). This range represents an erosional remnant of a volcanic complex inside the Ohře Rift graben and can be divided into four lithostratigraphic units (Cajz 2000), of which the most important are the lowermost Ústí Formation (36–26 Ma) composed of olivine-basaltic effusions confined to the rift valley and the overlying Děčín Formation (31–25 Ma) composed mostly of explosive tephritic to trachybasaltic volcanic products of a composite volcano. The two younger formations (Dobrná Formation and Štrbice Formation) are not present at Dlouhý vrch Hill.

In the area of Skalice, the Ústí Formation is absent and the Děčín Formation overlies the Santonian marine sandstones of the Merboltice Formation (87–85 Ma), which is the youngest preserved unit of the Bohemian Cretaceous Basin. Here, the lowermost unit of the Děčín Formation is represented by several superimposed bodies of dense volcaniclastic rock of tephritic composition, as revealed by a recent geological survey (Fig. 2). Conversely, the quartzites are not developed at places where other rock types (lahars and lavas) form the base of the Děčín Formation (Cajz 2004), or where the base of the volcanic complex is represented by the Ústí Formation.

Although the paleorelief can hardly be reconstructed in full detail, the documented examples of redeposited pre-volcanic sediments, intravolcanic fluvial sediments (Děčín Formation) and quartzite occurrences, indicate the presence of a shallow, roughly N–S-trending valley before the deposition of the lowermost preserved products of the České středohoří Mts volcanic complex.

The Skalice quartzite body is subhorizontal, ca. 10 m thick, visible in numerous outcrops at ca. 460 m a.s.l. along the southern slopes of Dlouhý vrch Hill. Gravitationally redeposited quartzite blocks can be found over a much larger area.

The relation of the Merboltice Formation sandstones to the overlying quartzites is clearly a parental one, as is shown by their similar composition and gradual transition. The presence of well-developed positive-graded bedding and common cross-bedding in the quartzites, contrasting with the generally massive Merboltice Formation sandstones, suggests fluvial reworking of the Cretaceous detrital material. Discrete, small basins in the České středohoří Mts were filled with fluvial to lacustrine sands, sometimes correlated with the Staré Sedlo Formation of the Sokolov Basin (Knobloch et al. 1996). The age of this process is indicated by fossil plant remnants in the quartzites. These were first studied by Engelhardt (1876) and include species, like *Steinhauera subglobosa* Presl *in* Sternberg, *Eotrigonobalanus furcinervis* (Rossmässler) Walther et Kvaček, *Sterculia labrusca* (Unger) Unger, or *Daphnogene cinnamomea* (Rossmässler) Knobloch. The presence of the first mentioned taxon indicates pre-Oligocene deposition of the parental sand, most probably in the Middle to Late Eocene (Knobloch & Konzalová 1998), i.e. at ca. 48–34 Ma.

As the upper contact of the quartzite body is not exposed in outcrops, a test pit was excavated for its detailed study at Dlouhý vrch Hill (Fig. 3), in an area not affected

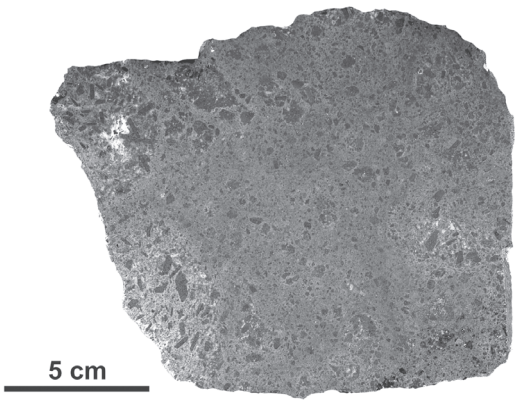

Fig. 2. Macrophotograph of the Dlouhý vrch tuff.

by mass movements. The Merboltice Formation (**Unit A** in Fig. 3) sandstones are white or light yellow, fine- to medium-grained, with imperfectly developed horizontal stratification. Some parts of the rock are brown due to the presence of iron oxyhydroxides. The gradual boundary against the overlying Skalice quartzites (**Unit B**) is due to a different intensity of cementation. The quartzites are white or light yellow, fine- to medium-grained. In the lowermost 7–8 m (**Subunit B1**), the quartzites have massive appearance, devoid of cavities. The quartzites in the topmost 2–3 m (**Subunit B2**) are rich in small cavities lined with quartz crystals, and locally contain abundant fossil flora. Cementation is massive, with no visible quartzite concretions, columns, pseudo-breccias or other features of preferred silica precipitation. Sedimentary structures documented in the ambience include trough cross-bedding and positive graded bedding. The boundary with the overlying dense volcaniclastics is wavy, represented by a sharp-based body of white, weakly consolidated, fine-grained kaolinitic sand with saponite, ca. 0.5 m thick — **Unit C**.

The sand is overlain by a suite of volcaniclastic rocks. In their rock type, they are endemic to Dlouhý vrch Hill and exceptional among other volcanics of the Děčín Formation. They are composed of juvenile and cognate volcanic clasts "welded" together by basic glass and can, therefore, be supposed to have originated as products of very hot pyroclastic flows ("ignimbrite") passing to lava flow rich in pyroclastic material of scoria ("clastic lava"), see Fig. 2. The presence of relatively fresh glass in this rock type is very rare compared to the Děčín Formation lavas, where the original glass is concentrated on the margins of volcanic bodies, is of much lower proportion, and is strongly devitrified, analcitized or zeolitized. If of pyroclastic origin, this rock type can be regarded as *ignimbrite s.l.* (according to earlier petrographic definitions), although this term is now being largely reserved for acidic rocks. To distinguish this rock from similar-looking products of lahars and common lavas, we use the term *dense tuff* or *tuff* in a non-genetic sense in the text below.

The fundamental discriminative feature between dense tuffs and lahars at Dlouhý vrch Hill is the much higher degree of solidification of the former. These tuffs are exposed in only several isolated outcrops and differ in terms of their average size, porosity, shape, colour and origin of clasts. This, and their alternation with regular terrestric lavas and lahar products, suggest that they represent several partly superimposed bodies. Lower bodies of dense tuff contain lithics of basanitic composition (Ústí Formation) while the upper ones contain only tephritic fragments. Three facies of the dense tuff can be distinguished in the test pit and its vicinity (**Units D–F**).

A layer approximately 0.2 m thick is present at the base, with entrained irregular fragments/lenses of light consolidated kaolinitic sand dispersed in clay matrix showing peperite-like structure — **Unit D**.

Tuff in **Unit E**, ca. 1.5–2 m thick, is altered to brown-grey kaolinite, smectite and illite clay. Sparse lithic clasts,

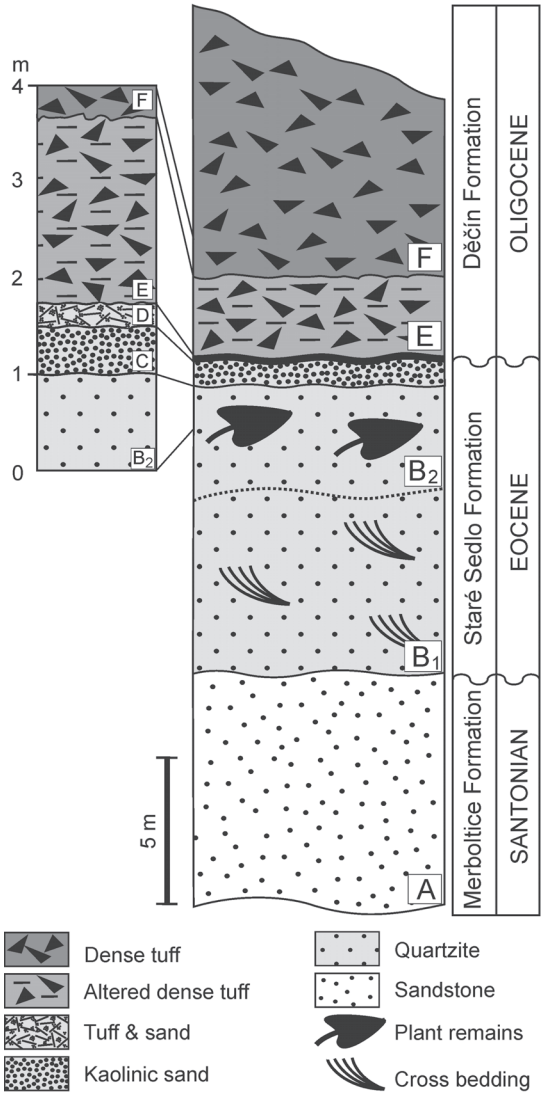

Fig. 3. Vertical section across the boundary between the Skalice quartzite and the overlying Dlouhý vrch tuff as seen in the excavated test pit. For the test-pit location see Fig. 1. Capital letters A–F correspond to individual lithological units discussed in the text.

up to 5 cm in size, are also altered in a similar style. Quartz grains entrained from the underlying sand are present, but not as common as in Unit D.

Solid dense tuff in **Unit F** exposed above the test pit contains lithic clasts and a high proportion of glass in the groundmass. Large clasts represent cognate lava fragments and juvenile scoriaceous material. Large volcanic clasts are mostly subangular to suboval, 10–20 cm in average size, but considerably smaller and larger clasts can also be found. The boundary with the altered tuff below has not been reached by excavation. No prominent grading was observed in the section, with the exception of the absence of large volcanic clasts in Unit E in the test-pit. No fiamme, glass shards, columnar cooling joints or degassing pipes were observed in any of the outcrops.

Methods

Rock samples (sandstone, quartzite, dense tuff) were taken from the excavated test pit as well as from other outcrops and quartzite blocks in the area. A total of 15 polished sections were made for petrographic study. These were studied in transmitted and polarized light using an optical microscope. Scanning cathodoluminescence (SEM-CL) with Cameca SX 100 electron microprobe was performed at the Geological Survey of the Slovak Republic in Bratislava (analyst V. Kollárová), using accelerating voltage 20 kV, beam current 60 nA for the discrimination of different silica generations. The surfaces of quartz grains from the weakly consolidated sand were observed using the CamScan CS 3400 scanning electron microscope at the Czech Geological Survey in Prague (analyst K.D. Malý, 15 kV, 150 μA). The mineral phases of hand-separated grains from the sandstone and quartzite were identified using the Philips X'pert X-ray diffractograph at the Institute of Geology, Academy of Sciences of the Czech Republic in Prague (analyst J. Dobrovolný), using CuKα radiation, generator voltage of 40 kV, generator current of 40 mA, $2\Theta = 2–75°$, scanning speed of $0.02° \cdot s^{-1}$. The discriminated types of secondary quartz were analysed for the contents of Al, Na, K, Fe and Ti using the Cameca SX 100 microprobe at the Institute of Geology, Academy of Sciences of the Czech Republic in Prague (analyst V. Böhmová, 15 keV, 10 nA). The same device was used for the analyses of the dense tuff. Whole-rock wet analyses were performed in the Laboratories of the Czech Geological Survey in Prague (analysts V. Janovská, J. Šikl) for the main rock types.

Skeletal densities (densities of solid phase) were determined by means of He pycnometry at the Institute of Chemical Process Fundamentals, Academy of Sciences of the Czech Republic in Prague, using the Accupyc 1330 Micrometrics helium pycnometer (analyst H. Šnajdaufová), with 5 cycles of purging, equlibration rate of 0.58 Pa/s = 0.005 psig/min.). Statistical evaluation provides accuracy down to 0.001 g/cm^3. Measurements of the total intrusion volume, median and average pore radii, bulk density were performed at the same institute using a high-pressure mercury Micrometrics AutoPore III porosimeter (analyst H. Šnajdaufová). This instrument allows high-pressure mercury intrusion of up to 400 MPa (corresponding to pore radii of 1.5 nm).

Petrology

Sandstone, Merboltice Formation (Unit A)

The sandstone is well sorted, with subangular to rounded detrital grains from 0.1–0.2 (70 %) to 0.3–0.5 mm in size (30 %). They are composed of quartz (90 %), kaolinized feldspar (K-feldspar >> plagioclase), micas and heavy minerals (magnetite, ilmenite). Monocrystalline quartz grains, 60 % with undulatory extinction, prevail over polycrystalline grains, which constitute 15–20 %. Some pores are partly filled with kaolinite (Fig. 4A). The overall degree of cementation is low: diagenetic quartz Q_1 forms irregular growth zones, 10–30 μm thick, but does not exceed 5 % of total sample volume. In SEM-CL images, Q_1 growth zones are dark and with no visible fabric; therefore, no signs of their possible corrosion can be identified.

Skalice quartzite (Unit B)

The quartzites contain detrital grains composed of quartz (95 %), micas and a very small proportion of heavy minerals. Detrital grains are subangular to rounded, and their size distribution is similar to that of the Merboltice Formation sandstone: 0.1–0.2 mm (90 %) and 0.3–0.5 mm (10 %). The proportion of polycrystalline quartz grains is 3–10 %, 70–80 % of monocrystalline grains show undulatory extinction. Some 20 % of grains, especially finer ones, show concave surfaces indicative of corrosion. Quartz grains are overgrown with quartz, constituting 20–40 % of the rock volume.

In the upper part of the Skalice quartzite body (Subunit B2), the main silica phase is megaquartz and microquartz (in small cavities). Grey varieties of quartzite B2 also contain aggregates of hematite crystals on diagenetic quartz. The lower part of the Skalice quartzite body (Subunit B1) contains only megaquartz. The proportion of quartz cement increases upwards within the whole quartzite body, and the increase in relative porosity in the same direction is only due to the elevated cavernosity in quartzite B2. Three types of quartz cement were distinguished:

1 — Minor growth zones of diagenetic quartz Q_1, 10–50 μm thick, were observed directly on the grains, much like in the sandstone. These overgrowths are mostly invisible in transmitted light, but are discernible in SEM-CL images. They are of uneven thickness, generally darker than the younger Q_2 overgrowths, and usually do not completely overgrow the grains. This indicates some corrosion before the formation of Q_2. Q_1 zones are homogeneous, unbanded, but display ghosts of fibrous textures in some places, which might indicate opal-CT/chalcedony recrystallization.

2 — Younger Q_2 overgrowths, found in quartzites only, are up to 100 μm thick and completely enclose the detrital

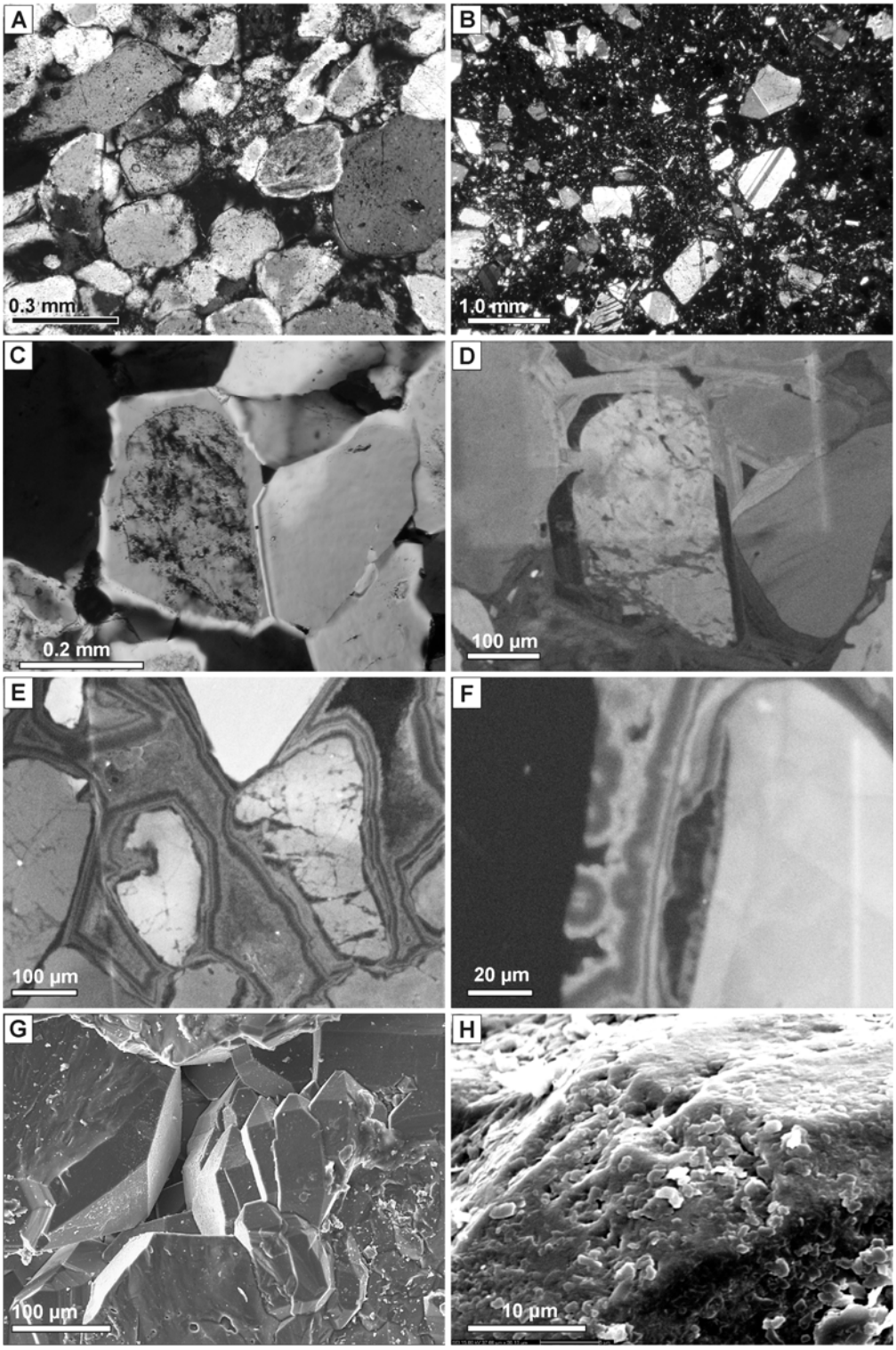

Fig. 4. A — Sandstone of the Merboltice Formation, Unit A. Crossed nicols, Sample 312. Quartz grains are partly cemented by kaolinite clay. **B** — Dense tuff overlying the quartzite, Unit F. Crossed nicols, Sample 308. Larger clinopyroxene xenocrysts and smaller plagioclase xenocrysts in the tephritic glassy groundmass. **C, D** — Quartzite, Subunit B1, Sample 306. C — Crossed nicols, dark core of the grain in the centre of the photo represents detrital quartz grain rich in fluid inclusions. In contrast to the core, the overgrowth zone of this grain is free of fluid/solid inclusions. D — SEM-CL image. The grain in the centre is overgrown by a dark Q_1 zone, isopachous growth bands Q_{2A} and euhedral growth zones Q_{2B}. **E, F** — Quartzite, Subunit B2. SEM-CL images, Sample 303. E — Euhedral to isopachous Q_2 bands and topmost bright zone of microquartz Q_3. F — Spherulitic Q_2 growth bands on a tourmaline grain (black). **G** — Quartzite, Subunit B2. SEM image, Sample 303. Microquartz Q_3 crystals filling a triple-junction cavity. **H** — Kaolinic sand, Unit C. SEM image, Sample 315. Corroded surface of a detrital quartz grain.

grains. These overgrowths are formed almost exclusively by megaquartz. The proportion of grains with crystal faces increases upwards in the section, reaching 80 % in Subunit B2.

In the lower part of the Skalice quartzite body (Subunit B1), this type is represented by ~50 μm thick quartz overgrowths, apparently homogeneous in transmitted light. In SEM-CL images, Q_{2A} and Q_{2B} types of fabric can be identified. The Q_{2A} fabric consists of multiple (max. 15) isopachous growth bands, 1–2 μm thick, alternating bright and dark, roughly copying grain surfaces and their Q_1 linings (Fig. 4E). They may represent recrystallized amorphous silica coatings. Growth bands of the Q_{2B} fabric are euhedral to subhedral, mostly grow over those of Q_{2A}, sometimes being separated by a distinct truncation surface. At least 9 bands can be distinguished, each 3–5 μm thick, and fill all the voids in the rock. Rarely, Q_{2B} bands are overgrown by Q_{2C} bands of the same character as the Q_{2A} bands.

In the upper part of the Skalice quartzite body (Subunit B2), this type consists of six quartz growth bands, each 5–20 μm thick, visible in transmitted light. The lowermost three bands are sometimes fused. In SEM-CL images, these bands are manifested by alternating dark and bright colours. The lowermost four bands often show saw-like patterns caused by the growth of minute quartz crystals, while the topmost — and the broadest — two bands display less acute angles which may indicate recrystallized amorphous silica coatings. Very rarely, the topmost two bands were observed to form spherules up to 35 μm in diameter on surfaces of tourmaline detrital grains (Fig. 4F).

3 — The youngest Q_3 generation consists of microquartz (crystals 30–150 μm) and is present in Subunit B2 only. The crystals are euhedral (Fig. 4G). They commonly grow on the topmost zone of Q_2 quartz, with the serrated contact indicating some degree of corrosion of the latter. The thickest microquartz layers were observed on the surfaces of small cavities at triple junctions of detrital grains. This type was commonly found in small cracks in the quartzite.

Weakly consolidated sand (Unit C)

The sand of Unit C at the contact with the tuff is well sorted, dominated by subangular to rounded quartz grains, 0.1–0.2 mm in size. Surface morphology indicates grain corrosion (Fig. 4H). Interstices are filled with coarse kaolinite (crystals 10–20 μm in diameter) and saponite.

Solid dense tuff (Unit F)

The rock contains pyroxene and plagioclase xenocrysts and volcanic fragments in the tephritic glassy groundmass. Xenocrysts of clinopyroxenes (0.8–3 mm in size) are automorphic, zoned, those of possible cumulate origin form crystals with pressure lamellae and reaction rims up to 0.1 mm thick. Clinopyroxene xenocrysts enclose automorphic grains of titanian magnetite (0.05–0.2 mm) and ilmenite. Magnetite grains have concave, corrosional margins with glass embayments. Plagioclase xenocrysts (0.15–0.2 mm) are vitrified and corroded along cleavage planes. Enclaves of iddingsitized olivine(?) are rare.

Dark fresh glass dominates the groundmass and also lines pyroxene xenocrysts and volcanic fragments. Its proportion locally reaches 40 % of rock volume. Besides glass, the groundmass also includes clinopyroxene microphenocrysts (0.1–0.4 mm) and fragments of larger xenocrysts. Small acicular and skeletal anorthoclase crystallites, 0.02–0.05 mm in size, are ubiquitous in most samples (ca. 25 % of groundmass) and completely surrounded by glass.

Volcanic fragments (~30 vol. %) form clasts, 2–3 mm in diameter. They contain clinopyroxene phenocrysts (0.5–0.7 mm), plagioclase (max. 0.5 mm), opaque minerals and holocrystalline groundmass. Some of the fragments have voids filled with zeolites and silica (opal), and some of them have partly zeolitized groundmass.

Chemical composition

Bulk analyses of main rock types are shown in Table 1 and microprobe analyses of the solid tuff are summarized in Table 2.

Skalice quartzite

Variations in the Al, Na, K, Ti and Fe contents in secondary quartz overgrowths were studied on electron microprobe in both quartzite subunits, B1 and B2, along grain-to-overgrowth profiles. The contents of K, Ti and Fe were mostly below the detection limits of 0.025 wt. %, 0.020 wt. % and 0.100 wt. %, respectively. Profiles with Al and Na contents representative for each subunit are shown in Fig. 5.

Clear differences were observed in Al contents, for which the detection limit was 0.016 wt. %. Al contents in detrital grains depend on the presence of fluid inclusions, inclusions of feldspars, micas and clay minerals. Overgrowths in quartzite B1 show only a small variation in Al, with its contents not exceeding 0.020 wt. %. Here, Al contents correspond to the luminescence colours, with lighter bands being richer in Al compared to darker bands. In quartzite B2, however, a steady increase in Al contents can be seen from the grains outwards, with values in excess of 0.020 wt. % in the youngest Q_2 bands. A clear increase in Na contents to exceed the detection limit (0.019 wt. %) was observed from the detrital grains outwards.

These trends of Al and Na distribution are, however, not reflected in the bulk-rock composition of the B1 and B2 quartzite. The grey, hematite-containing variety of quartzite B2 shows elevated Fe content (0.23 wt. %) in the bulk-rock analysis.

Solid dense tuff and argillized tuff

The bulk composition of the dense tuff need not reflect the parental magma composition as a result of the air-sorting of pyroclastic material during transport and alteration. Solid tuff from Skalice plots in the field of alkali basalt in

Table 1: Representative bulk analyses of the main rock types.

	Sandstone **Unit A** Sample 312 wt. %	**Quartzite** **Unit B1** Sample 307 wt. %	**Quartzite (dark variety)** **Unit B2** Sample 306TM wt. %	**Quartzite (light variety)** **Unit B2** Sample 306SV wt. %	**Altered dense tuff** **Unit E** Sample 314 wt. %	**Fresh dense tuff** **Unit F** Sample 308 wt. %
SiO_2	93.59	99.52	99.34	99.50	53.66	43.87
TiO_2	0.09	0.07	0.07	0.07	1.98	2.55
Al_2O_3	3.59	0.12	0.11	0.13	13.22	14.67
Fe_2O_3	0.08	< 0.01	0.23	0.04	9.60	9.89
MgO	0.04	< 0.01	0.01	0.01	1.79	3.98
MnO	< 0.001	< 0.001	< 0.001	< 0.001	0.073	0.190
CaO	0.01	< 0.01	0.02	0.02	1.20	11.58
Na_2O	0.10	0.02	0.02	0.03	0.26	1.54
K_2O	1.76	0.04	0.03	0.04	1.24	1.78
P_2O_5	0.03	0.03	0.02	0.02	0.18	0.66
LOI	0.63	0.18	0.16	0.13	6.29	6.26
$H2O^-$	< 0.05	< 0.05	< 0.05	< 0.05	10.33	3.02
Total	99.92	99.98	100.01	99.99	99.82	99.99

Table 2: Average microprobe analyses of the main phases in the solid ignimbrite, Sample 308.

	Glass (groundmass) *n = 21* wt. %	**Anorthoclase crystallites** *n = 10* wt. %	**Ti-magnetite** *n = 9* wt. %	**Plagioclase** *n = 6* wt. %	**Pyroxene** *n = 19* wt. %
SiO_2	50.21	51.86	0.15	57.15	47.04
TiO_2	2.12	1.55	18.80	0.17	2.87
Al_2O_3	18.79	19.37	4.24	26.26	6.10
Fetot	8.06*	4.68*	71.10*	0.53	7.77
MgO	1.92	1.30	4.75	0.03	12.11
MnO	0.28	0.17	0.96	0.03	0.23
CaO	9.13	3.75	0.11	8.52	22.13
Na_2O	1.92	6.61	–	5.93	0.75
K_2O	1.67	4.23	–	0.92	0.02
Cr_2O_3	0.05	0.08	0.04	–	0.03
BaO	0.04	0.12	–	0.22	0.02
F	0.26	0.19	–	–	–
Cl	0.01	0.19	–	–	–
Total	94.46	94.10	100.15	99.76	99.07

* recalculated to ferric iron

the TAS (total alkali vs. silica) diagram (Table 1). As revealed by microprobe analyses (Table 2), glass in the groundmass of the solid tuff is of prevailing basaltic composition, with SiO_2 values ranging between 47.9 and 52.2 wt. % and total alkali content between 2.5 and 5.3 wt. %. The alkalinity index (Na_2O+K_2O/Al_2O_3) varies within the range of 0.14–0.27. Both sodic and potassic glasses are present ($K_2O/Na_2O = 0.17–2.23$). Average *Mg*-number [MgO/(MgO + 0.15 FeO)×100] for glass corresponds to the value of 64.3 (55.5–75.0).

Small anorthoclase crystallites are scattered in the glass in most samples of the solid tuff. In microprobe analyses, their composition is contaminated by Ca, Fe and Ti from the surrounding groundmass glass. Not only alkali contents (average 10.8 wt. % K_2O+Na_2O) but also Al contents (average 19.4 wt. % Al_2O_3) exceed those in the glass. Sodium slightly predominates over potassium in most crystallites, although extreme K_2O/Na_2O ratios were also encountered (0.03–6.65). Plagioclase phenocrysts are mostly of andesine to labradorite composition. Magnetite in the solid tuff is enriched in Ti, with 14.3–22.4 wt. % TiO_2.

To characterize the style of alteration, the chemistry of tuff from Unit F was compared with that of argillized tuff from Unit E. Argillized tuff is markedly depleted in Ca, Na, Mg and P and enriched in Si (Table 1), thus indicating the decomposition of plagioclase and pyroxene, with Al being locked in the newly formed kaolinite. Although some release of silica from glass and plagioclase can be expected, the true extent of the silica depletion is obscured by the admixture of detrital quartz grains. This explains the extremely high Si contents in the argillized tuff.

Density and porosity measurements

Samples of sandstone (Unit A, Sample 312) and quartzites from the lower part (Subunit B1, Sample 306) and upper part of the Skalice quartzite body (Subunit B2, Sample 303) were analysed for skeletal densities (densities of solid phase) and bulk densities, plotting their pore-size distributions. Skeletal densities were also determined for altered dense tuff (Unit E, Sample 314) and fresh dense tuff (Unit F, Sample 313). The data are summarized in Table 3 and Fig. 6.

Both quartzite samples show much lower total porosities than the sandstone, with the highest porosity reduc-

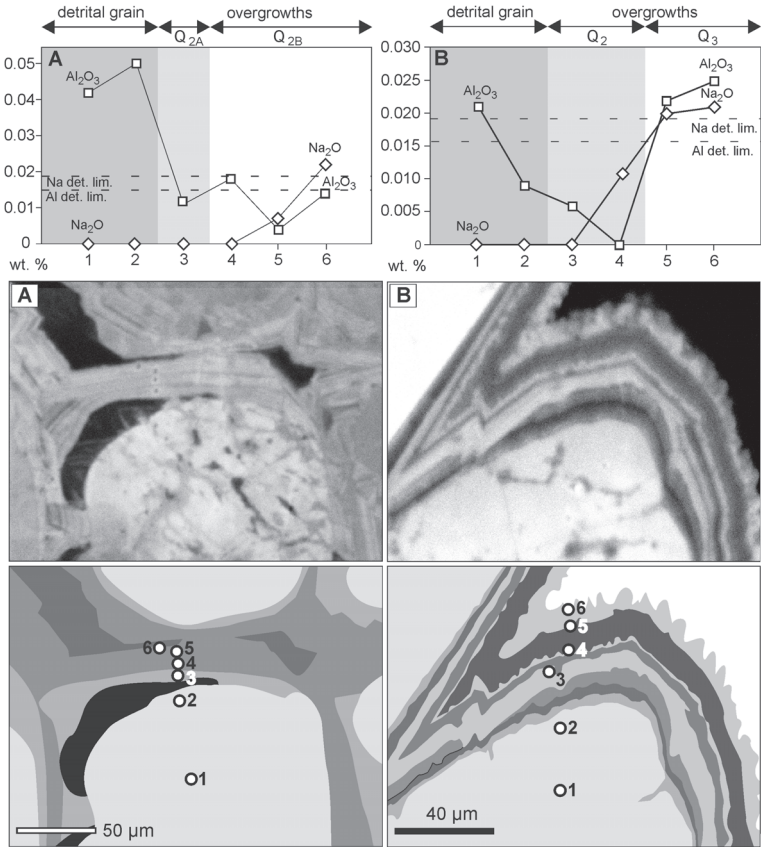

Fig. 5. Al_2O_3 and Na_2O contents in detrital quartz grains and their overgrowths, and the corresponding SEM-CL photos with analytical profiles. **A** — Lower part of the Skalice quartzite body (Subunit B1). **B** — Upper part of the Skalice quartzite body (Subunit B2).

tion found in quartzite of Subunit B2 (porosity 3.84 %). As shown by the pore-size distribution diagrams (Fig. 6), the infrequent large corrosive pores (3–50 µm) in all quartzites have no secondary mineral fills. Nevertheless, quartzites of Subunit B2 — unlike those of Subunit B1 — are characterized by almost complete filling of pores in the size category of 0.1 to 2 µm with quartz of the youngest Q_3 generation.

Discussion

Dense tuff alteration: devitrification or hydrothermal desilicification?

The time gap of over 4 Myr between the Eocene fluvial deposition of fossiliferous sand and the Late Oligocene onset of tephritic volcanic activity (Děčín Formation) must have brought relative uplift and partial erosion of the tectonic block at Dlouhý vrch Hill, as shown by the local absence of the Ústí Formation products. The former river channels may have been abandoned and the Dlouhý vrch tuff was deposited on dry land. This is suggested by the absence of signs of interaction with water, such as chilling and quenching phenomena or fumarolic pipes, in the outcrops and by the absence of palagonitization or fumarolic alteration in microscopic scale. Breccia with peperite-like structure in Unit D is viewed as a product of mechanical incorporation of loose sediment into the basal portions of the pyroclastic flow.

The average values of SiO_2 and alkalis (48.4 wt. % and 3.7 wt. %, respectively) for the studied volatile-free tuff, differ from 43.7 wt. % SiO_2 and 5.2 wt. % alkalis in average volatile-free tephrite of the Bohemian Massif (Shrbený 1995), and project into the field of alkali basalt in the TAS diagram. The discrepancy between the tephritic habitus and mineral content of the solid tuff and its basaltic chemistry is explained by the loss of alkalis and by the high proportion of glass (50.2 wt. % SiO_2 on average), which adds extra silica to the contents typical of tephrites. A part of the free alkalis was locked in Na- and K-rich feldspar (anorthoclase) crystallizing from glass, but a significant part must have been removed from the rock. The presence of anorthoclase crystallites in relatively fresh glass suggests that these represent products of early post-emplacement devitrification induced by the thermodynamic instability of the glass (Cas & Wright 1987). Although fibrous silica is a common product of acidic glass devitrification, devitrification spherulites (cf. Lofgren 1971) are absent from the tuff. Chalcedony coatings in voids in the rock are, much like the zeolites, therefore rather attributed to downward seepage of rainwater through the tuff body. No major SiO_2 losses can be assumed during the devitrification stage as the newly formed anorthoclase is not depleted in silica relative to the glass.

The extensive argillization of the lowermost 1.7 to 2.2 m of the dense tuff body (Units D–E) and clayey sand (Unit C) was, however, associated with a much more extensive solute transport than the devitrification process observed in Unit F. Therefore, it must have entailed some degree of fluid involvement. In the absence of surface water, the most probable solute carrier was rainwater percolating through the tuff. The argillization either post-dated, or was synchronous with, the devitrification stage. Volcanic glass was transformed into a mixture of smectite, kaolinite and illite, which implies considerable losses of SiO_2. Large-scale Ca and Na removal during the argillization process is compatible with the decomposition of plagioclase and clinopyroxene. This transformation could have proceeded in two steps, with smectite crystallization at temperatures of 20–150 °C (Aoki et al. 1996) and its subsequent hydrothermal alteration into a mixture of kaolinite and illite at approximately 80–100 °C. The latter reaction took place in an alkaline environment with a concomitant release of additional SiO_2. The increase in vol-

Table 3: Results of helium pycnometry and mercury porosimetry of the main rock types.

	Sandstone Unit A Sample 312	**Quartzite Unit B1** Sample 306	**Quartzite Unit B2** Sample 303	**Altered dense tuff Unit E** Sample 314	**Fresh dense tuff Unit F** Sample 313
Skeletal density ($kg \cdot m^{-3}$)	2650	2660	2641	2629	2696
Bulk density ($kg \cdot m^{-3}$)	1891	2538	2540	no data	no data
Median pore radius (10^{-9} m)	3.6	4.7	4.0	no data	no data
Average pore radius (10^{-9} m)	114.8	110.5	24.4	no data	no data
Porosity (%)	28.64	4.59	3.84	no data	no data

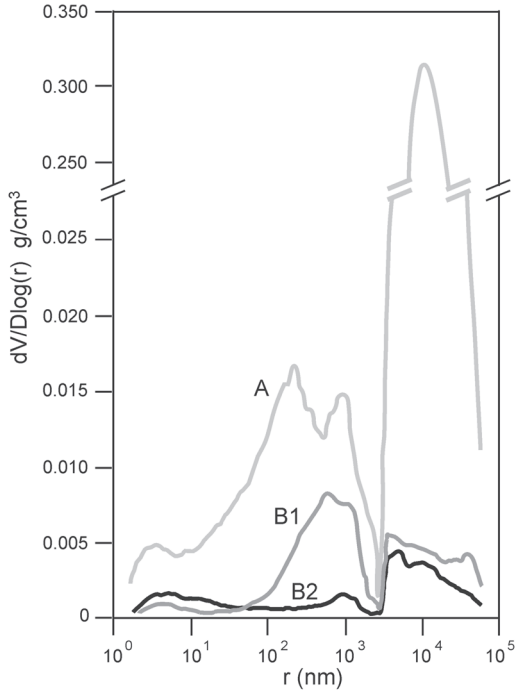

Fig. 6. Diagrams of differential pore-size distribution in sandstone (Unit A) and quartzites from the lower part of the Skalice quartzite body (Subunit B1) and upper part of the Skalice quartzite body (Subunit B2).

ume associated with smectite alteration resulted in the crystallization of coarse kaolinite in Unit C below the tuff base. The late-stage timing of kaolinite and saponite crystallization in Unit C sand is supported by the fact that the unit must have been fully permeable for the hydrothermal fluids until the late stages of downward silica transport.

Mass balance and the source of silica

Knowledge of mineral transformations taking place during the tuff alteration permits us to calculate whether the tuff itself could serve as the source of secondary silica cement below its base. As the devitrification stage released possibly no silica from the tuff itself, only the argillization/silicification stage is considered. The observation that the quartzites are developed only beneath the dense tuff allows us to eliminate the horizontal component of solute transport in the mass balance calculations, and to consider only mass fluxes in a vertical section. As precise calculations are impossible due to the admixture of detrital quartz in Units D–E and the unknown degree of grain corrosion in Unit C, the amounts of transported silica can merely be estimated.

Assuming that the proportions of glass, plagioclase and pyroxene (the main phases subject to decomposition) in the solid tuff are 3.5 : 2.5 : 4, together constituting 85 % of the rock (based on thin sections and mineral chemistry), and that these phases in the argillized dense tuff are completely transformed into kaolinite with 46.5 wt. % SiO_2, the mass of released SiO_2 on a unit area of the tuff/sand contact can be calculated:

$$m_{loss} = (0.85A/100) \cdot \rho_{tuff} \cdot T_t \quad (1)$$

where A is the weighted average of the difference in SiO_2 contents in these three mineral phases and kaolinite in wt. % (available excess silica), ρ_{tuff} is the skeletal density of the argillized dense tuff, and T_t is the thickness of the argillized dense tuff.

The potential amount of available silica is approximately 4.2 wt. %, skeletal density of the laboratory sample of argillized dense tuff is 2630 $kg \cdot m^{-3}$, and the approximate thickness of the argillized dense tuff is 2 m (Units D–E). Under such conditions, the mass of the released SiO_2 can be estimated at 188 $kg \cdot m^{-2}$.

The gains of silica in the quartzite (Unit B) underlying the tuff can be quantified as follows:

$$m_{gain} = (P_s - P_q) \cdot \rho_{silica} \cdot T_q \quad (2)$$

where P_s and P_q are relative porosities of unaltered sandstone and quartzite, respectively, ρ_{silica} is the density of the newly formed silica phases in the quartzite, and T_q is the thickness of the quartzite. Relative porosities measured in laboratory samples are 0.286 for sandstone, 0.046 for B1 quartzite, and 0.038 for B2 quartzite. The ρ_{silica} value of 2600 $kg \cdot m^{-3}$ was used for B1 quartzite, dominated by quartz overgrowths, while the density of 2100 $kg \cdot m^{-3}$ was used for B2 quartzite, dominated by recrystallized opal overgrowths. Thicknesses T_q of B1 and B2 quartzite are 7.5 m and 2.5 m, respectively. The mass of the newly precipitated SiO_2 can then be estimated at 4680 $kg \cdot m^{-2}$ for Subunit B1 and 1302 $kg \cdot m^{-2}$ for Subunit B2, namely 5982 $kg \cdot m^{-2}$ in total.

A comparison of the approximate supply (188 $kg \cdot m^{-2}$) vs. gain (5982 $kg \cdot m^{-2}$) of silica, however imprecise these estimations may be, suggests that the tuff could not serve as a sole source for the secondary silica cement in the

quartzite, even if all the main mineral phases were completely kaolinized. The main process of silica production for the quartzite must therefore be seen in the alkaline dissolution of quartz grains beneath the pyroclastic flow.

The solubility of quartz in the sand beneath the tuff could have been controlled by higher alkali contents in fluids generated during the alteration of feldspar, clay minerals and alkali glass (Levandowski et al. 1973). Nevertheless, quartz is equally dissolved by fluids of normal pH at elevated temperatures (Rimstidt 1997). Also, the presence of organic acids in fluids of normal pH increases the dissolution rate of quartz considerably even at 25 °C (Bennett et al. 1988). All these factors can be held responsible for quartz dissolution in the sand beneath the Dlouhý vrch tuff.

Silicification process in sand

Silica cement precipitated in pure quartzose sand after disintegration and redeposition of the underlying Merboltice Formation sandstone. The high purity of the target lithology, devoid of kaolinized feldspar and clay minerals, is a necessary pre-requisite for the quartz overgrowths to form (McBride 1989). The presence of albite, talc and amphibole reported from feldspathic and clayey sandstones at their contact with volcanic rock (Brauckmann & Füchtbauer 1983; McKinley et al. 2001) was not encountered in the Skalice quartzites.

The succession of the silicification process as documented by microscopic observations is illustrated in Fig. 7. The earliest, sporadic quartz overgrowths Q_1 are developed also in the non-silicified Merboltice Formation sandstones, which suggests that they are products of pre-Eocene burial diagenesis. The main phase of silicification with the formation of subhedral overgrowths in quartzite B2 and isopachous and euhedral overgrowth in quartzite B1 relates to the circulation of fluids activated by the emplacement of the hot pyroclastic flow. Petrographic differences between B1 and B2 quartzites can be most easily explained by their different positions relative to the groundwater table. Descending fluids in B2 were providing silica for broad overgrowths discernible in CL images, where each zone/band represents a separate batch of fluid seeping from the tuff to its basement. In contrast, the zone of B1 quartzites, lying below the groundwater table, precipitated silica of much more homogeneous chemical composition, producing compound sets of mostly bright isopachous growth bands with less variation in Al contents. Conversion of amorphous silica precipitation into quartz precipitation in the B1 quartzite can be explained either in terms of decreasing silica concentration in fluids or by the presence of impurities (clay minerals, e.g.) on quartz grains that prevented early crystallization of quartz. Later recrystallization of amorphous silica into quartz in the whole profile may be due to the sinking of the groundwater table during progressive incision of relief or due to the dehydration upon sediment burial.

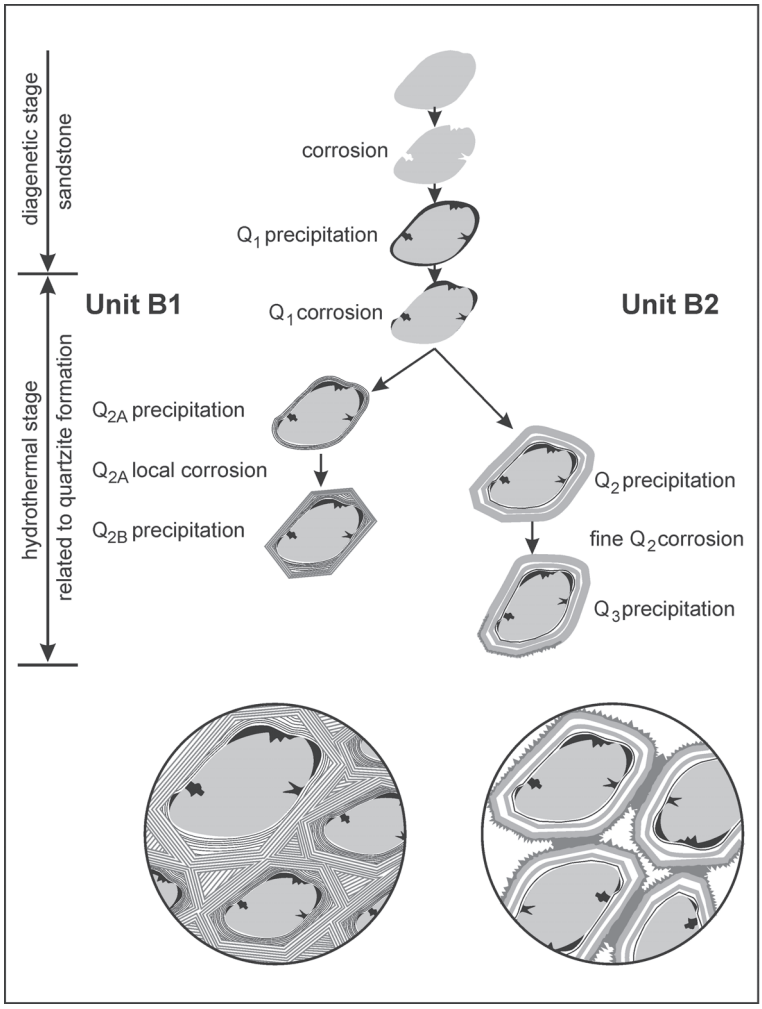

Fig. 7. A schematic diagram of the succession of silicification stages in the Skalice quartzite. Note the different silicification histories of its lower part (Subunit B1) and upper part (Subunit B2). The distinction is explained by their respective positions below and above the groundwater table.

The isopachous character of the growth bands of Q_{2A} from the lower part of the Skalice quartzite body allows us to speculate on early fluids with high SiO_2 concentration and high amounts of impurities, giving rise to poorly crystalline silica cement. A release of fluids with such parameters seems to be compatible with the process of volcanic glass alteration in the dense tuff. Subsequently formed euhedral growth zones of Q_{2B} in the lower part of the Skalice quartzite body and Q_2 in its upper part precipitated, on the other hand, from relatively pure fluids with lower SiO_2 concentration, compatible with the process of smectite transformation into kaolinite and illite in the basal portion of the tuff. Precipitation of euhedral quartz was probably concomitant with the recrystallization of earlier, poorly crystalline phases into megaquartz.

The last stage, characterized by Q_3 precipitation, was preceded by the corrosion of Q_2 quartz in quartzite B2. The clarity and small size of Q_3 quartz crystals indicate a steady fluid chemistry (lower SiO_2 concentration, low content of impurities) but a certain decline in the flushing rate.

Diagnostic features for volcanic alteration vs. silcretization of quartz arenites

Quartzite bodies developed in the sands of the Staré Sedlo Formation in other parts of the Ohře Rift graben bear signs of pedogenic silcretization: distinct vertical profiles with pseudo-brecciation horizons, vertical succession of silica phases, and TiO_2 accumulation. The approximately coeval Skalice quartzites, much smaller in areal extent, were believed to be a result of the same silicification process by earlier authors (e.g. Malkovský 1985).

In fact, the Skalice quartzites lack the features characteristic of pedogenic silcretes summarized by Thiry (1997). Instead, they can be briefly described by a simple three-storey vertical profile with decreasing intensity of corrosion and increasing intensity and variety of silica precipitation in a downward direction (Fig. 7). No inheritance of micromorphological features is observed in the uppermost horizons as an indication of the 'progressively sinking profile' of Thiry (1997). In contrast, the Skalice quartzites share many petrographic features indicative of groundwater silcretes, the best described example of which are the Fontainebleau quartzites (Thiry & Maréchal 2001). Especially the isopachous quartz overgrowths developed on detrital grains and rarely on euhedral overgrowths, most probably representing recrystallized opal coatings, indicate precipitation in stagnant or slowly circulating silica-supersaturated groundwater. However, no elongated or air-foil morphologies of quartzite bodies suggesting preferred fluid flow direction are visible, and the Skalice quartzite rather forms one thick, tabular body with no internal structuring.

The Fontainebleau model presumes a long-distance silica supply by groundwater, the silica oversaturation of which results from alteration of clay minerals in the overlying formation, and only occasional dissolution within the quartzite body itself is admitted. In contrast, the Skalice quartzites show very strong dissolution in the topmost portion (loose sand with corroded grain surfaces) and medium dissolution in the upper part of the quartzite body (dissolution cavities in quartzite B2). This, and the fact that the tuff itself could not produce enough silica for the cement in quartzite, documents a progressive downward Si transport from Unit E to Unit B as far as to the B1/B2 quartzite boundary. Below this boundary, quartzite B1 displays only rare, mild corrosion features. On the basis of these observations, the B1/B2 boundary should be viewed as the local groundwater table at the time of the silicification process.

The process of Si leaching from the tuff and the underlying sand and its deposition around the groundwater table must have been rather rapid. As suggested by the presence of post-dissolution hydrothermal kaolinite in Unit C sand below the tuff base, the silica transport must have been completed before cooling of the pyroclastic flow.

In summary, the process of the Skalice quartzite formation can be described as rapid silica mobilization induced by hydrothermal alteration of a tephritic pyroclastic flow and sudden heating and alkalization of the sand in the proximity of a groundwater table. Such hydrothermal process clearly outpaces the classical process of groundwater silcrete formation driven by mixing of meteoric water with silica-rich groundwater and silica precipitation in water discharge areas. Therefore, the Skalice quartzite body should be regarded as a hydrothermal quartz deposit, despite its geometry defined by the course of the groundwater table at the time of the pyroclastic flow emplacement.

Conclusions

The horizontally lying body of the Skalice quartzites near Litoměřice, Ohře Rift graben, shows no signs of supergene origin. On the contrary, its spatial association with the overlying body of the Dlouhý vrch tuff, the presence of hydrothermal kaolinite in sand at the quartzite/tuff boundary, and the lack of features characteristic for silcretes suggest silica mobilization beneath the tuff layer during its deposition. The documented vertical section across the tuff/quartzite boundary, petrographic observations and chemical analyses of the main rock types indicate three stages of interaction between the tuff and its basement during a progressive temperature decrease:

1 — dealkalization of the tuff synchronous with glass recrystallization (origin of anorthoclase crystallites), resulting in quartz grain corrosion beneath the tuff base; the released silica was deposited in the form of opal coatings on quartz grains deeper in the profile (Subunit B1);

2 — hydrothermal desilicification (smectitization of volcanic glass) and continued dealkalization in the basal part of the tuff body connected with massive silicification of the sand beneath the tuff base; origin of euhedral quartz cement deeper in the profile (Subunit B1) and opal coatings in shallower parts of the profile (Subunit B2);

3 — transformation of smectite in the basal part of the tuff body into kaolinite and illite; kaolinite crystallized on top of the sand profile prevents further fluid movement and solute exchange between the tuff and the sand.

The boundary between the shallower, loosely cemented and partly corroded quartzite B2 and the deeper, densely cemented quartzite B1, can be identified with the groundwater table at the time of quartzite formation. As the mass balance calculations imply the silica supply from the tuff itself would not be sufficient for the Skalice quartzite formation in its total thickness of ca. 10 m. Additional topography-controlled quartz-grain dissolution in the underlying sands is also shown by the frequent signs of corrosion, especially above the groundwater table.

The style of cementation in the Skalice quartzite was — to a certain degree — controlled by the paleorelief (tuff base) and the depth of the groundwater table. In this sense, it can be considered a special type of a groundwater silcrete. The

distinction from the groundwater silcrete model of Thiry & Maréchal (2001) lies in the short-term, heat-driven silica mobilization, and in the short-distance, essentially vertical silica transport. The thoroughly documented case of the hydrothermal Skalice quartzite is to warn against hasty genetic interpretations of horizontal quartzite bodies where the overlying strata have not been preserved.

Acknowledgments: The authors wish to thank J.K. Novák and J. Ulrych (Inst. Geology AS CR Prague) for their help in the processing of electron microprobe analyses. Porosity measurements were kindly provided by O. Šolcová (Inst. Chem. Process Fundamentals AS CR Prague). The study of sandstone silicification is supported by the Grant Agency of the Academy of Sciences CR, Project No. A3013302 and falls within the Academic Research Plan AV0Z 30130516.

References

Aoki S., Kohyama N. & Hotta H. 1996: Hydrothermal clay minerals found in sediment containing yellowish-brown material from the Japan Basin. *Mar. Geol.* 129, 331–336.

Bennett P.C., Melcer M.E., Siegel D.I. & Hassett J.P. 1988: The dissolution of quartz in dilute aqueous solutions of organic acids at 25 °C. *Geochim. Cosmochim. Acta* 52, 1521–1530.

Brauckmann F.J. & Füchtbauer H. 1983: Alterations of Cretaceous siltstones and sandstones near basalt contacts (Nugssuaq, Greenland). *Sed. Geol.* 35, 193–213.

Cas R.A.F. & Wright J.V. 1987: Volcanic successions modern and ancient. A geological approach to processes, products and successions. *Allen and Unwin*, London, 1–528.

Cajz V. 2000: Proposal of lithostratigraphy for the České středohoří Mts. volcanics. *Bull. Czech Geol. Surv.* 75, 1, 7–16.

Cajz V. 2004: Contribution to volcanology of the Litoměřice area, North Bohemia. *Zpr. Geol. Výzk. v Roce 2003*, 16–19 (in Czech with English abstract).

Dittler E. & Hibsch J.E. 1928: Über basaltische Zersetzungsprodukte und die Bildung von Quarzit. *Tschermaks Mineral. Petrogr. Mitt.* 39, 1, 2, 45–75.

Engelhardt H. 1876: Tertiärpflanzen aus dem Leitmeritzer Mittelgebirge. Die Tertiärpflanzen des Süßwassersandsteins von Schüttenitz. *Nova Acta Leop.-Carol. Akad. Naturforsch.* 38, 4, 397–414.

Guidry S.A. & Chafetz H.S. 2003: Anatomy of siliceous hot springs: examples from Yellowstone National Park, Wyoming, USA. *Sed. Geol.* 157, 71–106.

Knobloch E. & Konzalová M. 1998: Comparison of the Eocene plant assemblages of Bohemia (Czech Republic) and Saxony (Germany). *Rev. Palaeobot. Palynol.* 101, 29–41.

Knobloch E., Konzalová M. & Kvaček Z. 1996: Die obereozäne Flora der Staré Sedlo-Schichtenfolge in Böhmen (Mitteleuropa). *Rozpr. Čes. Geol. Úst.* 49, 1–260.

Kužvart M. 1965: Weathering of quartzites covered by basalt tuffs in north-western Bohemia. *Acta Universitatis Carolinae — Geologica* 3, 227–236.

Levandowski D.W., Kaley M.E., Silverman S.R. & Smalley R.G. 1973: Cementation in Lyons Sandstone and its role in oil accumulation, Denver Basin, Colorado. *Amer. Assoc. Petrol. Geol. Bull.* 57, 2217–2244.

Lofgren G. 1971: Spherulitic textures in glassy and crystalline rocks. *J. Geophys. Res.* 76, 5635–5648.

Malkovský M. 1985: Quartzites. In: Malkovský M. (Ed.): Geology of the North Bohemian Brown Coal Basin and its surroundings. *Ústř. Úst. Geol., Acad.*, Praha, 324–326 (in Czech).

Malkovský M. 1991: Genetic types of silicification of Upper Cretaceous and Tertiary sediments of northwestern Bohemia. In: Souček J. (Ed.): Rocks in Earth sciences. *Univ. Karlova Praha, Karolinum*, Praha, 63–68 (in Czech).

McBride E.F. 1989: Quartz cement in sandstones: A review. *Earth Sci. Rev.* 26, 69–112.

McKinley J.M., Worden R.H. & Ruffell A.H. 2001: Contact diagenesis: The effect of an intrusion on reservoir quality in the Triassic Sherwood Sandstone Group, Northern Ireland. *J. Sed. Res.* 71, 484–495.

Prodehl C., Mueller S. & Haak V. 1995: The European Cenozoic rift system. In: Olsen K.H. (Ed.): Continental Rifts: Evolution, structure, tectonics. *Developments in Geotectonics* 25. Elsevier, Amsterdam, 133–212.

Rimstidt J.D. 1997: Quartz solubility at low temperatures. *Geochim. Cosmochim. Acta* 61, 2553–2558.

Shrbený O. 1995: Chemical composition of young volcanites of the Czech Republic. *Czech Geol. Surv. Spec. Pap.* 4, 1–54.

Summerfield M.A. 1983: Petrography and diagenesis of silcrete from Kalahari Basin and Cape Coastal Zone, Southern Africa. *J. Sed. Petrology* 53, 895–909.

Thiry M. 1997: Continental silicifications: a review. In: Paquet H. & Clauer N. (Eds.): Soils and sediments. Mineralogy and geochemistry. *Springer-Verlag*, Berlin, 191–221.

Thiry M. & Maréchal B. 2001: Development of tightly cemented sandstone lenses in uncemented sand: example of the Fontainebleau Sand (Oligocene) in the Paris Basin. *J. Sed. Res.* 71, 473–483.

Thiry M. & Milnes A.R. 1991: Pedogenic and groundwater silcretes at Stuart Creek Opal Field, South Australia. *J. Sed. Petrology* 61, 111–127.